

A POD reduced order unstructured mesh ocean modelling method for moderate Reynolds number flows

F. Fang^{a,*}, C.C. Pain^a, I.M. Navon^b, G.J. Gorman^a, M.D. Piggott^a, P.A. Allison^a, P.E. Farrell^a, A.J.H. Goddard^a

^a Applied Modelling and Computation Group, Department of Earth Science and Engineering, Imperial College London, Prince Consort Road, London SW7 2BP, UK

^b Department of Scientific Computing, Florida State University, Tallahassee, FL 32306-4120, USA

ARTICLE INFO

Article history:

Received 7 May 2008

Received in revised form 14 November 2008

Accepted 17 December 2008

Available online 4 January 2009

Keywords:

Reduced-order modelling

Ocean model

Finite element

Unstructured adaptive mesh

POD

ABSTRACT

Herein a new approach to enhance the accuracy of a novel Proper Orthogonal Decomposition (POD) model applied to moderate Reynolds number flows (of the type typically encountered in ocean models) is presented. This approach develops the POD model of Fang et al. [Fang, F., Pain, C.C., Navon, I.M., Piggott, M.D., Gorman, G.J., Allison, P., Goddard, A.J.H., 2008. Reduced-order modelling of an adaptive mesh ocean model. *International Journal for Numerical Methods in Fluids*. doi:10.1002/flid.1841] used in conjunction with the Imperial College Ocean Model (ICOM), an adaptive, non-hydrostatic finite element model. Both the velocity and vorticity results of the POD reduced order model (ROM) exhibit an overall good agreement with those obtained from the full model.

The accuracy of the POD-Galerkin model with the use of adaptive meshes is first evaluated using the Munk gyre flow test case with Reynolds numbers ranging between 400 and 2000. POD models using the L^2 norm become oscillatory when the Reynolds number exceeds $Re = 400$. This is because the low-order truncation of the POD basis inhibits generally all the transfers between the large and the small (unresolved) scales of the fluid flow. Accuracy is improved by using the H^1 POD projector in preference to the L^2 POD projector. The POD bases are constructed by incorporating gradients as well as function values in the H^1 Sobolev norm. The accuracy of numerical results is further enhanced by increasing the number of snapshots and POD bases. Error estimation was used to assess the effect of truncation (involved in the POD-Galerkin approach) when adaptive meshes are used in conjunction with POD/ROM. The RMSE of velocity results between the full model and POD-Galerkin model is reduced by as much as 50% by using the H^1 norm and increasing the number of snapshots and POD bases.

© 2008 Elsevier Ltd. All rights reserved.

1. Introduction

The resolution of ocean models is one of the most important issues in the development of global circulation models. Over the last decades an important contribution to improving the resolution of ocean models has involved the introduction of unstructured meshes. Unstructured, dynamically-adaptive mesh models can efficiently resolve global, basin, regional and small-scale flow structures. Adaptive meshing methods recently introduced to 4D-Var data assimilation are capable of producing a best estimate model solution by fitting a numerical simulation to observational data over both space and time (Fang et al., 2005, 2006). The use of adaptive meshes allows the accuracy of both the forward and inverse calculations to be optimised dynamically.

However, a major hurdle in the implementation of 4D-Var data assimilation for ocean modelling is the large dimensionality (typi-

cally in the range 10^6 – 10^8) of these problems. Computing the cost function and its gradient results in high memory and computational costs, requiring the integration of both the forward model and its adjoint. To overcome this difficulty, reduced-order modelling presents a powerful concept enabling a representation of the dynamics of large-scale systems on a smaller number of degrees of freedom. Proper Orthogonal Decomposition (POD), in combination with the Galerkin projection procedure has been shown to provide an efficient means of generating reduced order models (Holmes et al., 1998; Luo et al., 2007a,b). The Galerkin projection on POD subspace directly transforms the PDE (Partial Differential Equation) system of the incompressible Navier–Stokes equations to a system of ODE (Ordinary Differential Equation), requiring greatly reduced computational effort. This technique identifies the most energetic modes in a time-dependent system, providing a means of obtaining a low-dimensional description of the system's dynamics.

POD has been widely and successfully applied to numerous fields, including signal analysis and pattern recognition (Fukunaga, 1990), fluid dynamics and coherent structures (Holmes et al., 1998; Lumley, 1967; Aubry et al., 1988; Willcox and Peraire, 2002) and

* Corresponding author. Tel.: +44 207594 9322.

E-mail address: f.fang@imperial.ac.uk (F. Fang).

URL: <http://amcg.ese.imperial.ac.uk> (F. Fang).

image reconstruction (Kirby and Sirovich, 1990). The practical use of the POD approach has also been extended to large scale complex flow dynamics such as ocean modelling (Luo et al., 2007a; Cao et al., 2006) and the four-dimensional variational (4D-Var) data assimilation (Cao et al., 2006; Robert et al., 2005; Hoteit et al., 2006; Daescu and Navon, 2008). Furthermore, the POD approach has been incorporated in an unstructured mesh finite element ocean model (Fang et al., 2008a,b) which includes an ability to simultaneously resolve both small and large scale ocean flows (as they evolve), and improved representation of bathymetry/coastlines.

The price of the low-dimensionality, however, entails a lack of stability especially for transitional and turbulent flows (Iollo et al., 2000; Couplet et al., 2005; Noack et al., 2005; Galletti et al., 2004; Gloerfelt, 2006). This either restricts reduced order models to a narrow range of parameters or to a short-time integration span. High Reynolds number ocean flows exhibit dynamics on a wide range of scales. They display a combination of organised or coherent structures – associated with the phase-averaged/spatially phase-correlated components that exhibit the most evident structure – and apparently disorganised or incoherent structures associated with the random components. The energy transfer/interaction between the different coherent/inherent structure flows plays an important role in high Reynolds number flows. Low-order truncation of the POD basis, however, inhibits transfers between the large and small (unresolved) scales of the fluid flow. As a consequence there is a lack of dissipation in POD-ROM and the reduced order model may diverge. Therefore, at higher Reynolds numbers – where more kinetic energy is constrained within the smaller scales – more POD snapshots as well as more bases should be retained for a realistic representation (Galletti et al., 2004).

To improve the accuracy of POD-Galerkin models, the effect of these unresolved modes must be included to provide an insight into the turbulent energy. Various calibration methods have been developed to enhance the stability of POD-Galerkin models (Couplet et al., 2005; Gloerfelt, 2006; Galletti et al., 2005; Pastoor et al., 2008). The calibration terms can include an eddy-viscosity function, as well as constant or/and linear terms. These calibration terms are computed by minimising a cost functional defined as either: the difference between the amplitude coefficients predicted by the calibrated POD and those from the POD; or a weak constraint functional, where the constraints are calibrated POD equations and are enforced by introducing Lagrange multipliers or adjoint variables. The effect of pressure gradients for incompressible flow is also the primary source for the lack of dissipation (Noack et al., 2005; Galletti et al., 2004; Rempfer et al., 2003). Noack et al. (2005) and Galletti et al. (2004) proposed a quadratic model (based on a Poisson problem) and a linear model (based on a least squares procedure) for the pressure calculation, respectively.

Herein the effect of the truncated modes is first evaluated when adaptive meshes are used in conjunction with POD. To recover the effect of the truncated bases (usually the small scales), a dissipative term is directly included in the construction of the POD basis (Iollo et al., 2000). POD is defined in the H^1 Sobolev norm rather than in the L^2 norm. This incorporates gradients as well as function values into the definition of POD. The stability of the POD-Galerkin model is evaluated in a Munk gyre tested with Reynolds numbers ranging between 400 and 2000.

2. POD approach in an adaptive mesh ocean model

2.1. Imperial College Ocean Model

The POD-Galerkin reduced order model presented here was developed for use with the Imperial College Ocean Model (ICOM)

(Fang et al., 2008a). ICOM is capable to simulate oceanic flow on a wide range of horizontal and vertical scales as well as modelling large-scale oceanic flows by using dynamically-adaptive meshes (using high resolution in localised regions to resolve small-scale features which affect large scale processes) (Pain et al., 2005; Ford et al., 2004). Surface conforming finite elements are used for coastline and ocean floor topography. The model employs 3D anisotropic mesh adaptivity to resolve and reveal fine scale features as they develop while reducing resolution elsewhere. Being non-hydrostatic it can cope with steep topography. It is also unconstrained by a rigid lid to permit accurate modelling of surface tides in shallow on-shelf regions, as well as the interaction between barotropic and baroclinic tides and other flows. In addition, it takes advantage of domain decomposition methods (DDM) in order to run on distributed memory parallel machines. The model consists of the 3-D continuity and non-hydrostatic Boussinesq equations:

$$\nabla \cdot \mathbf{u} = 0, \quad (1)$$

$$\frac{\partial \mathbf{u}}{\partial t} = F(\mathbf{u}) - \nabla p, \quad (2)$$

where

$F(\mathbf{u}) = -\mathbf{u} \cdot \nabla \mathbf{u} - f \mathbf{k} \times \mathbf{u} - \rho \mathbf{g} \mathbf{k} + \nabla \cdot \boldsymbol{\tau}$, $\mathbf{u} \equiv (u, v, w)^T \equiv (u_1, u_2, u_3)^T$ is the velocity vector, $\mathbf{x} \equiv (x, y, z)^T \equiv (x_1, x_2, x_3)^T$ are the orthogonal Cartesian coordinates, p is the perturbation pressure ($p := p/\rho_0$, ρ_0 is the constant reference density), f represents the Coriolis inertial force, \mathbf{g} represents the acceleration due to gravity, ρ is the perturbation density ($\rho := \rho/\rho_0$), and $\mathbf{k} = (0, 0, 1)^T$. The stress tensor $\boldsymbol{\tau}$ is used to represent viscous terms. The pressure variable is split into the non-geostrophic and geostrophic parts which are solved separately. This allows the accurate representation of hydrostatic/geostrophic balance (for details see, Ford et al., 2004).

2.2. Proper Orthogonal Decomposition

Let the model variables $\{V_k(\mathbf{x}, t_k)\}$ (e.g. velocity $\mathbf{u} = (u, v, w)$ and pressure p) be a set of snapshots sampled at the defined check-points during the simulation $[t_1, \dots, t_k, \dots, t_K]$, where K is the number of snapshots assumed of uniform weight. The average of the ensemble of snapshots is defined as:

$$\bar{V} = \frac{1}{K} \sum_{k=1}^K V_k, \quad (3)$$

and the deviation from the mean of variables is defined as

$$v_k = V_k - \bar{V}, \quad (4)$$

The goal of POD is to find a set of orthogonal basis functions $\{\Phi_k\}$ such that it maximises

$$\frac{1}{K} \sum_{k=1}^K |\langle v_k, \Phi_k \rangle_{L^2}|^2, \quad (5)$$

subject to

$$\sum_{k=1}^K |\langle \Phi_k, \Phi_k \rangle_{L^2}|^2 = 1, \quad (6)$$

where $\langle \cdot, \cdot \rangle_{L^2}$ is the canonical inner product in L^2 norm. The approach introduced by Sirovich et al. (1987) is used to find an optimal set of basis functions Φ of the optimisation problem (5). The POD bases can be written as a linear combinations of the snapshots v_k :

$$\Phi_k = \sum_{k=1}^K y_k v_k; \quad 1 \leq k \leq K. \quad (7)$$

Therefore a $K \times K$ eigenvalue problem is solved

$$C y_k = \lambda_k y_k; \quad 1 \leq k \leq K, \quad (8)$$

where C is the $K \times K$ matrix with $C_{kl} = \frac{1}{K} \langle v_k, v_l \rangle (1 \leq k, l \leq K)$. The eigenvalues λ_k are real and positive and should be sorted in descending order. The eigenvectors y_k are orthogonal and are referred to as the POD basis vectors Φ_k . The k^{th} eigenvalue is a measure of the kinetic energy transferred within the k^{th} basis.

2.3. POD-Galerkin projection

The variables \mathbf{u} and p can be approximately expressed as an expansion of the first few POD basis functions $\{\Phi_{1,\mathbf{u}}, \dots, \Phi_{M,\mathbf{u}}\}$ and $\{\Phi_{1,p}, \dots, \Phi_{M,p}\}$, respectively:

$$\begin{aligned} \mathbf{u}(t, x, y, z) &= \bar{\mathbf{u}} + \sum_{m=1}^M \alpha_{m,\mathbf{u}}(t) \Phi_{m,\mathbf{u}}(\mathbf{x}), \\ p(t, x, y, z) &= \bar{p} + \sum_{m=1}^M \alpha_{m,p}(t) \Phi_{m,p}(\mathbf{x}), \end{aligned} \quad (9)$$

where $\bar{\mathbf{u}}$ and \bar{p} are the mean of the ensemble of snapshots for the variables \mathbf{u} and p , respectively, $\alpha_{m,\mathbf{u}}$ and $\alpha_{m,p} (1 \leq m \leq M)$ are the time-dependent coefficients to be determined; $\alpha_{m,\mathbf{u}}(0)$ and $\alpha_{m,p}(0)$ are the coefficients at the initial time level. Taking the POD basis function as the test function, then integrating over the computational domain Ω ,

$$\left\langle \frac{\partial \mathbf{u}}{\partial t}, \Phi_{m,\mathbf{u}} \right\rangle_{\Omega} = \langle F(\mathbf{u}), \Phi_{m,\mathbf{u}} \rangle_{\Omega} - \langle \nabla p, \Phi_{m,\mathbf{u}} \rangle_{\Omega}, \quad (10)$$

$$\langle \nabla \cdot \mathbf{u}, \Phi_{m,p} \rangle_{\Omega} = 0. \quad (11)$$

Substituting (9) into (10) and (11), the POD reduced order equations (ODEs) are then obtained:

$$\begin{aligned} \frac{\partial \alpha_{m,\mathbf{u}}}{\partial t} &= \left\langle F \left(\bar{\mathbf{u}} + \sum_{m=1}^M \alpha_{m,\mathbf{u}}(t) \Phi_{m,\mathbf{u}}(\mathbf{x}) \right), \Phi_{m,\mathbf{u}} \right\rangle_{\Omega} \\ &\quad - \left\langle \nabla \left(\bar{p} + \sum_{m=1}^M \alpha_{m,p}(t) \Phi_{m,p}(\mathbf{x}) \right), \Phi_{m,\mathbf{u}} \right\rangle_{\Omega}, \end{aligned} \quad (12)$$

$$\left\langle \left(\nabla \cdot \bar{\mathbf{u}} + \sum_{m=1}^M \alpha_{m,\mathbf{u}}(t) \Phi_{m,\mathbf{u}}(\mathbf{x}) \right), \Phi_{m,p} \right\rangle_{\Omega} = 0, \quad (13)$$

subject to the initial condition

$$\begin{aligned} \alpha_{m,\mathbf{u}}(0) &= ((\mathbf{u}(0, \mathbf{x}) - \bar{\mathbf{u}}(\mathbf{x})), \Phi_{m,\mathbf{u}}), \quad \alpha_{m,p}(0) \\ &= ((p(0, \mathbf{x}) - \bar{p}(\mathbf{x})), \Phi_{m,p}). \end{aligned} \quad (14)$$

2.4. Adaptive mesh technique in conjunction with POD

The use of dynamically-adaptive meshes has its advantage in resolving small and large flows simultaneously as dynamics evolve. However, this introduces a complication in the implementation of a POD-based reduced model for an adaptive model. When adaptive meshes are employed, the dimensional size of the variable vectors is different at each time level since the number of nodes varies during the simulation. Therefore the POD-ROM snapshots can be of different length at different time levels. In this study, a reference fixed mesh is adopted for the reduced model. The solutions from the original full model are interpolated from their own mesh onto the same reference fixed mesh at each time level, and then stored in the snapshots. The information at the snapshots is used to find an optimal set of basis functions. This allows the same length of base modes to be obtained at each time level of the numerical simulation. The resolution of the reference mesh and the interpolation errors between the two meshes (the adaptive mesh and the fixed reference mesh) may affect the accuracy of the POD simulation. The effect of the interpolation error has been investigated in our previous studies (Fang et al., 2008a,b). The comparison of POD re-

sults with the use of the different interpolation operators demonstrated that the accuracy of POD results can be improved by introducing the high order interpolation operators (Fang et al., 2008b). This will be explained and discussed through the applications presented below.

2.5. Geostrophic pressure

A deficit of dissipation in the energy budget, causing the POD-Galerkin model to drift, could be related to the pressure terms which appear at the boundaries of the computational domain (Noack et al., 2005; Galletti et al., 2004). To incorporate the pressure effects due to confinement, Noack et al. (2005) and Galletti et al. (2004) proposed a quadratic model (based on a Poisson problem) and a linear model (based on a least square procedure) for the pressure term, respectively,

In ocean modelling, the pressure term also plays an important role in the geostrophic balance. In this study, taking into account the role of the pressure term in both the POD-Galerkin model and the geostrophic balance, the pressure in the momentum equations is divided into two parts: $p = p_{ng} + p_g$. To accurately represent geostrophic pressure, its basis functions are split into two sets: Φ_{pgu} and Φ_{pgv} which are associated with the u - and v -velocity components. The geostrophic pressure can be obtained from a quadratic finite element representation while linear finite element representations are used for the velocity components. Furthermore, the geostrophic pressure can be represented by a summation of the two sets of geostrophic basis functions, which are calculated by solving the elliptic equations using a conjugate gradient iterative method (for details see, Fang et al., 2008a).

3. Stabilisation of reduced order model using a Sobolev H^1 norm

High Reynolds number ocean flows exhibit dynamics on a wide range of scales. They display a combination of organised or coherent structures associated with the phase-averaged/spatially phase-correlated components that exhibit the most evident structure and apparently disorganised or incoherent structures associated with the random components. The higher the Reynolds number, the broader this range of scales. The incoherent turbulence is typically of a time scale considerably smaller than that of the coherent structures. The lifetime of a coherent structure seems to decrease with increasing Reynolds number, when a structure appears to undergo fairly rapid evolutionary change through complex interactions (like tearing, fractional and partial pairings) or decay via turbulent diffusion by incoherent turbulence (Hussain, 1983). The distorted or subdivided structures find ways via mutual interactions to re-emerge and generate a new coherent structure. It is also noted that coherent and incoherent flows are not independent even if they are uncorrelated. Coherent structures both produce and spatially organise incoherent turbulence.

Reynolds shear stresses and the energy transfer/interaction between the different coherent/inherent structure flows play an important role in characteristics of moderate and high Reynolds number flows, i.e., the generation, evolution and decay of turbulent flows (e.g., eddies). It is not surprising that the POD reduced model derived using the Galerkin approach is not sufficiently accurate in reproducing the dynamics of higher Reynolds number flows since the truncation applied in the POD subspace inhibits transfers between the different scales of the fluid flow. The neglected POD modes correspond to small scale structures and introduce dissipative errors in the model. As a consequence, the system may lose its long-term stability. The stabilisation of a reduced order model can be achieved by introducing an artificial dissipation by using a Sobolev H^1 inner product norm, that is, the derivatives of the snap-

shots as well as those of the basis functions are included in the definition of POD (Iollo et al., 2000).

One seeks the POD basis function $\Phi = \Phi_1, \Phi_2, \dots, \Phi_K$ such that it maximises:

$$\frac{1}{K} \sum_{k=1}^K |\langle v_k, \Phi_k \rangle_{H^1}|^2 = \frac{1}{K} \sum_{k=1}^K \sum_{i=1}^{\mathcal{N}} (v_{k,i} \Phi_{k,i})^2 + \epsilon \frac{1}{K} \sum_{k=1}^K \sum_{i=1}^{\mathcal{N}} (\nabla v_{k,i} \cdot \nabla \Phi_{k,i})^2, \quad (15)$$

subject to

$$\sum_{k=1}^K |\langle \Phi_k, \Phi_k \rangle_{H^1}|^2 = 1, \quad (16)$$

where $v_k = (v_{k,1}, \dots, v_{k,\mathcal{N}})$ and $\Phi_k = (\Phi_{k,1}, \dots, \Phi_{k,\mathcal{N}})$ (\mathcal{N} being the number of nodes), ϵ is a coefficient to be chosen from dimensional analysis considerations (Iollo et al., 2000) (one may also guess the ϵ value). The POD basis function Φ_k can be calculated as in the L^2 case:

$$\Phi_k = \sum_{i=1}^{\mathcal{N}} y_{k,i} v_{k,i}; \quad 1 \leq k \leq K, \quad (17)$$

where y_k is obtained by solving the eigenvalue problem:

$$\mathcal{C} y_k = \lambda_k y_k; \quad 1 \leq k \leq K, \quad (18)$$

where \mathcal{C} is the $K \times K$ matrix with $\mathcal{C}_{k,l} = \frac{1}{K} (\langle v_k, v_l \rangle + \epsilon \langle \nabla v_k, \nabla v_l \rangle)$ ($1 \leq k, l \leq K$).

4. Application and discussion

The stability and accuracy of POD-Galerkin model using adaptive meshes is explored using the Munk gyre flow test case. By comparing the results between the POD-ROM and full models, the effect of the truncated modes is evaluated for Reynolds numbers in the range of 400–2000. To improve the stabilisation of numerical results, the POD bases are defined in a H^1 Sobolev norm. A comparison of results using the H^1 and L^2 POD results is carried out.

4.1. Description of the case: the Munk gyre

The POD-Galerkin reduced order model is tested in a computational domain of horizontal dimensions, 1000 km by 1000 km with a depth of $H = 500$ m. The wind forcing on the free surface is given by

$$\tau_y = \tau_0 \cos(\pi y/L), \quad \tau_x = 0.0, \quad (19)$$

where τ_x and τ_y are the wind stresses on the free surface along the x and y directions, respectively, and $L = 1000$ km. A maximum zonal wind stress of $\tau_0 = 0.1$ N/m is applied in the latitudinal (y) direction. The Coriolis terms are taken into account using the beta-plane approximation ($f = \beta y$) where $\beta = 1.8 \times 10^{-11}$ and the reference density is $\rho_0 = 1000$ kg/m.

The problem is non-dimensionalised with the maximum Sverdrup balance velocity

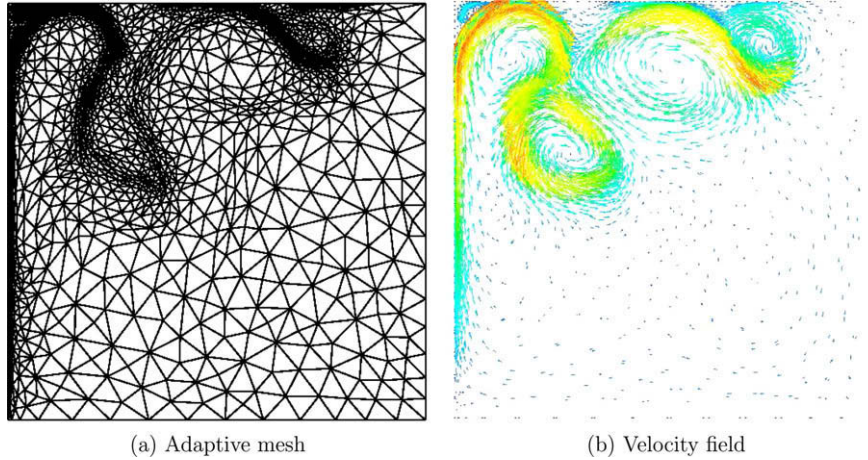


Fig. 1. Adaptive mesh and velocity field in the full model at time level $t = 150$ days ($Re = 2000$).

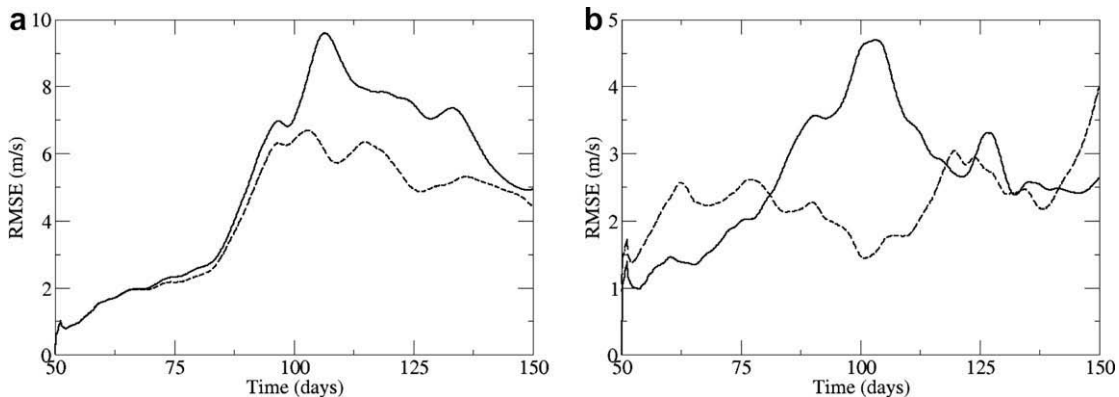


Fig. 2. RMSE of velocity results between the full and POD models (a) $Re = 800$ (41 snapshots with 30 POD bases); (b) $Re = 1200$ (81 snapshots with 60 POD bases). The solid line, with the use of the L^2 norm; the dashed line, with the use of the H^1 norm.

$$\beta H \rho_0 v = \frac{\partial \tau}{\partial y} \leq \frac{\tau_0 \pi}{L} \Rightarrow v \leq 3.5 \times 10^{-2} \text{ m/s}, \quad (20)$$

(and so the velocity scale $U = 3.5 \times 10^{-2}$ m/s is used here), and the length scale is $L = 1000$ km. Time is non-dimensionalised with $T = \frac{L}{U}$. The spin-up period is 0.1512 (50 days). The equilibrium state at 50 days is taken as the initial state for both the full and reduced models. The snapshots are collected from the results obtained in the full model during the simulation period [50, 150] days. The time step is 3.78×10^{-4} , equivalent to 3 h. Incorporating the beta-plane approximation yields a non-dimensional $\beta^* = \frac{L^2 \beta}{U} = 514.3$. The

non-dimensional wind stress (applied as a body force here averaged over the depth of the domain) takes the same cosine of latitude profile with $\tau_0^* = \frac{\tau_0 L}{(U^2 \rho_0 H)} = 163.3$. No-slip boundary conditions are applied to the lateral boundaries. The Reynolds number is defined as $Re = \frac{UL}{\nu}$.

The POD bases are constructed by snapshots which are obtained from the numerical solutions in the full model. To evaluate the effect of truncated modes, a range of moderate Reynolds numbers (400–2000) was used. Various numbers of snapshots and POD bases (dependent on the values of the Reynolds numbers tested)

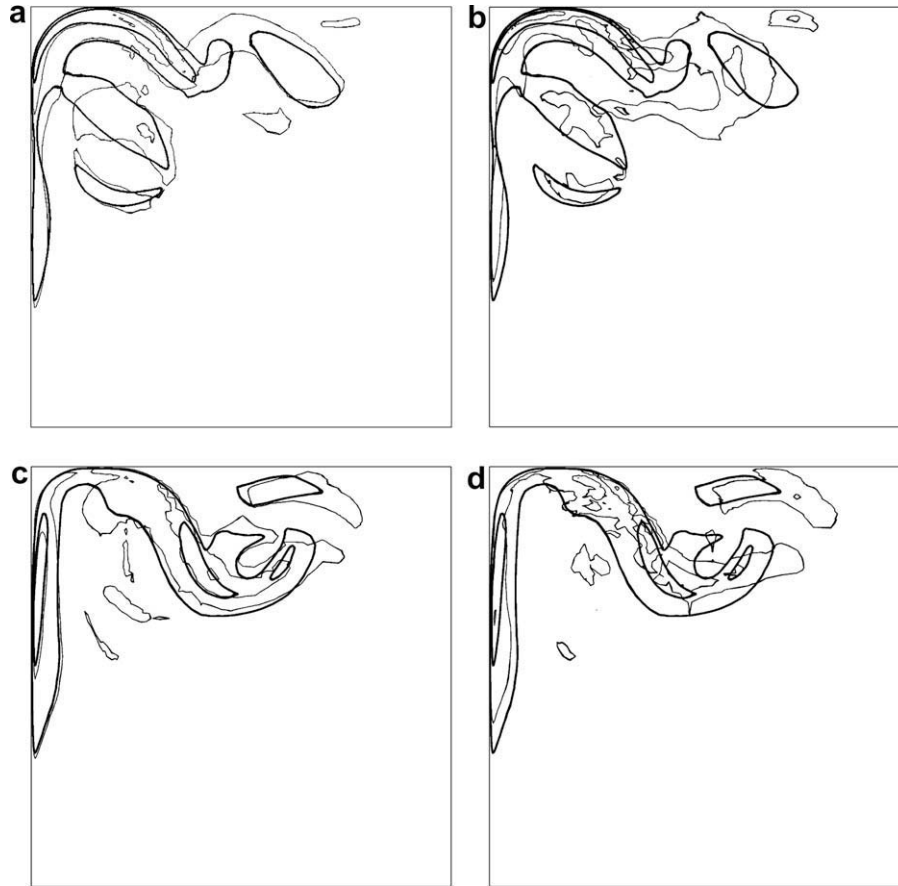


Fig. 3. Contour of velocity ($Re = 1200$) at time levels: (a) and (b) $t = 100$ days; (c) and (d) $t = 112.5$ days. Left panel: with the use of the H^1 norm; right panel: with the use of the L^2 norm (the thick lines: the full model; the thin lines: the POD model defined in H^1 . Eighty-one snapshots and 60 POD bases are chosen).

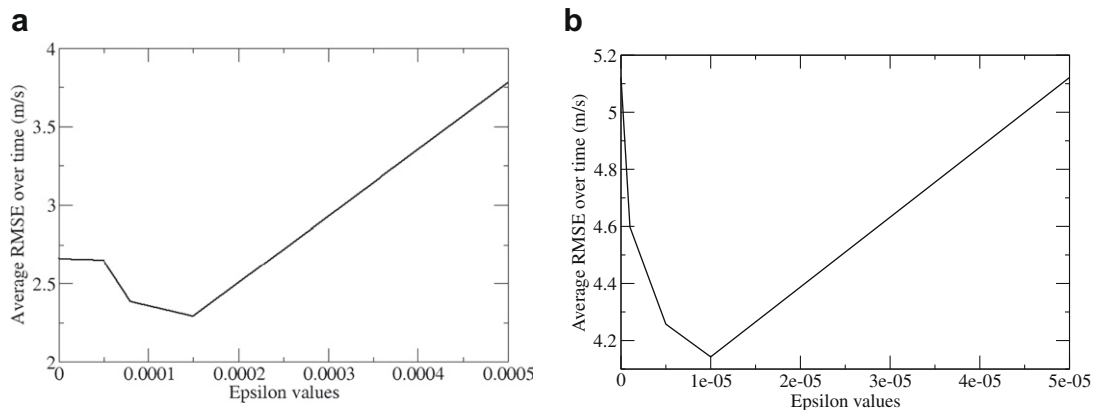


Fig. 4. Average (over time) RMSE of velocity results between the full model and the POD model defined in H^1 with different ϵ values: (a) $Re = 1200$; (b) $Re = 800$.

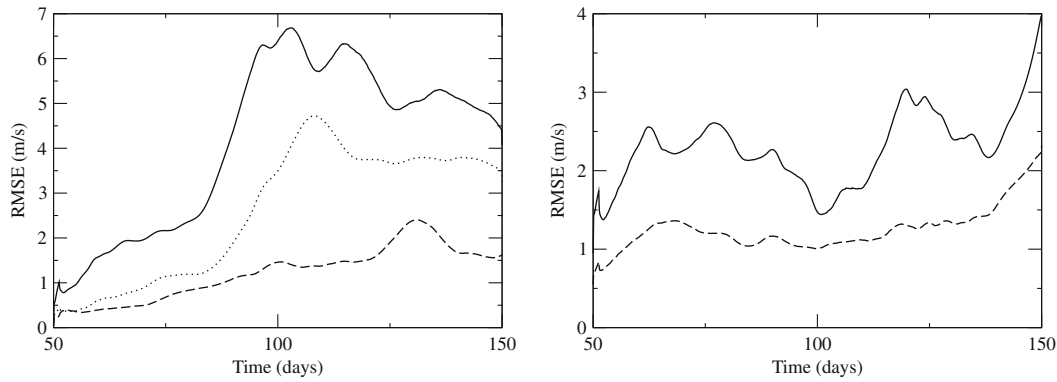


Fig. 5. RMSE of velocity results between the POD model and the full model with the uses of the piecewise linear (solid line), cubic (dashed line) and quadratic (dotted line) operators. Left panel: $Re = 800$ (41 snapshots with 30 POD bases for the linear and quadratic operators while 81 snapshots with 60 POD bases for the cubic operator); right panel: $Re = 1200$ (81 snapshots with 60 POD bases for all the interpolation operators).

for the velocity components u, v, w and the pressure p are chosen to capture more than 99% of energy.

An adaptive mesh is adopted in the full model. The mesh for the full model adapts every 19 time steps with maximum and

minimum mesh size of 0.2 and 0.001 (non-dimensional), respectively. The mesh was dynamically adapted according to the flow features. The adaptive mesh adopted (at time level $t = 150$ days) in the full model is shown in Fig. 1. To allow the same length of

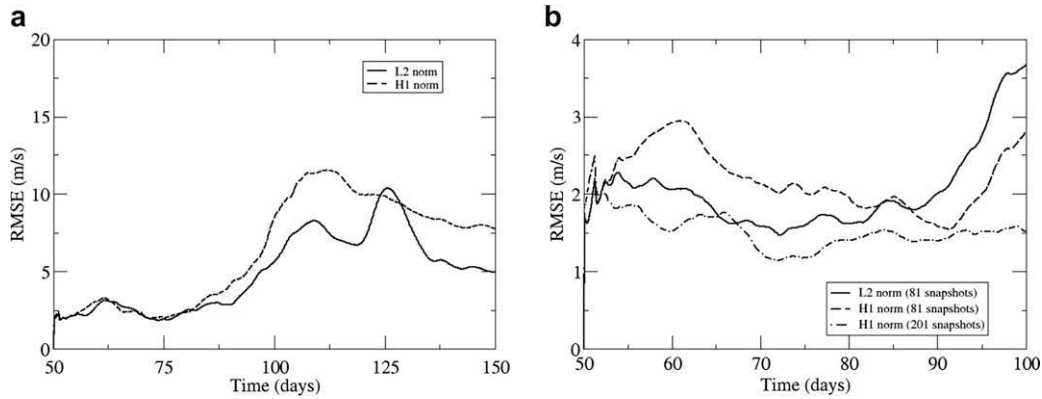


Fig. 6. RMSE of velocity results between the POD model and the full model ($Re = 2000$): (a) the POD model is derived based on snapshots obtained during a long period [50, 150] days (81 snapshots with 60 POD bases); (b) the POD model is derived based on snapshots obtained during a short period [50, 100] days (the solid line: 81 snapshots with 60 POD bases; the dashed line: 81 snapshots with 70 POD bases; the dot-dashed line: 201 snapshots with 100 POD bases).

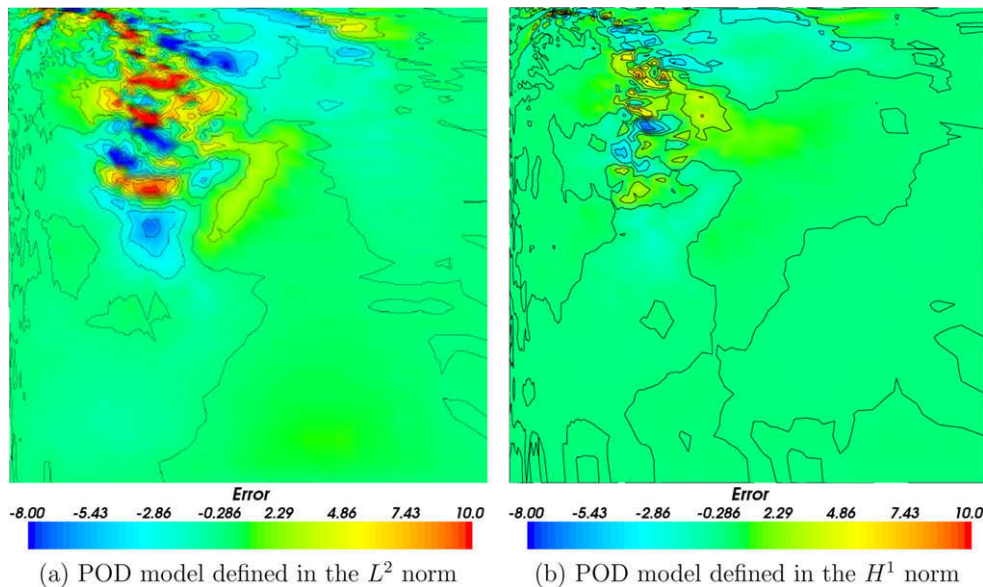


Fig. 7. Error in the velocity field from the POD reduced model ($Re = 2000$; unit: m/s) at time level $t = 150$ days: (a) with the use of L^2 (81 snapshots and 60 POD bases are chosen); (b) with the use of H^1 (201 snapshots and 100 POD bases are chosen).

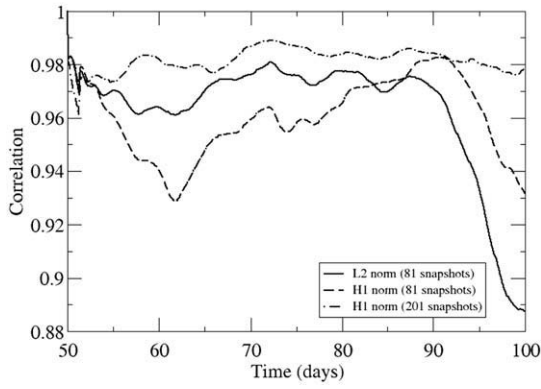


Fig. 8. Correlation of velocity results between the full model and the POD model defined in both the H^1 and L^2 ($Re = 2000$).

POD bases at the snapshots for the reduced order model, a reference fixed mesh is chosen. To build up the snapshots, the solutions from the full model are interpolated from the adaptive mesh onto the reference fixed mesh. The aim of this paper is to evaluate the effect of the truncated modes when adaptive meshes are used in conjunction with the POD-ROM. The POD-Galerkin model is derived using both the H^1 and L^2 norms. The root mean square error (RMSE) between the POD velocity solution and the true one at the time level n is used to estimate the error of the POD-ROM projection results:

$$RMSE^n = \sqrt{\frac{\sum_{i=1}^{\mathcal{N}} (U_i^n - U_{o,i}^n)^2}{\mathcal{N}}}, \quad (21)$$

where, U_i^n and $U_{o,i}^n$ are the vectors containing the POD velocity components and true ones at the node i , respectively, \mathcal{N} is the total number of nodes over the domain.

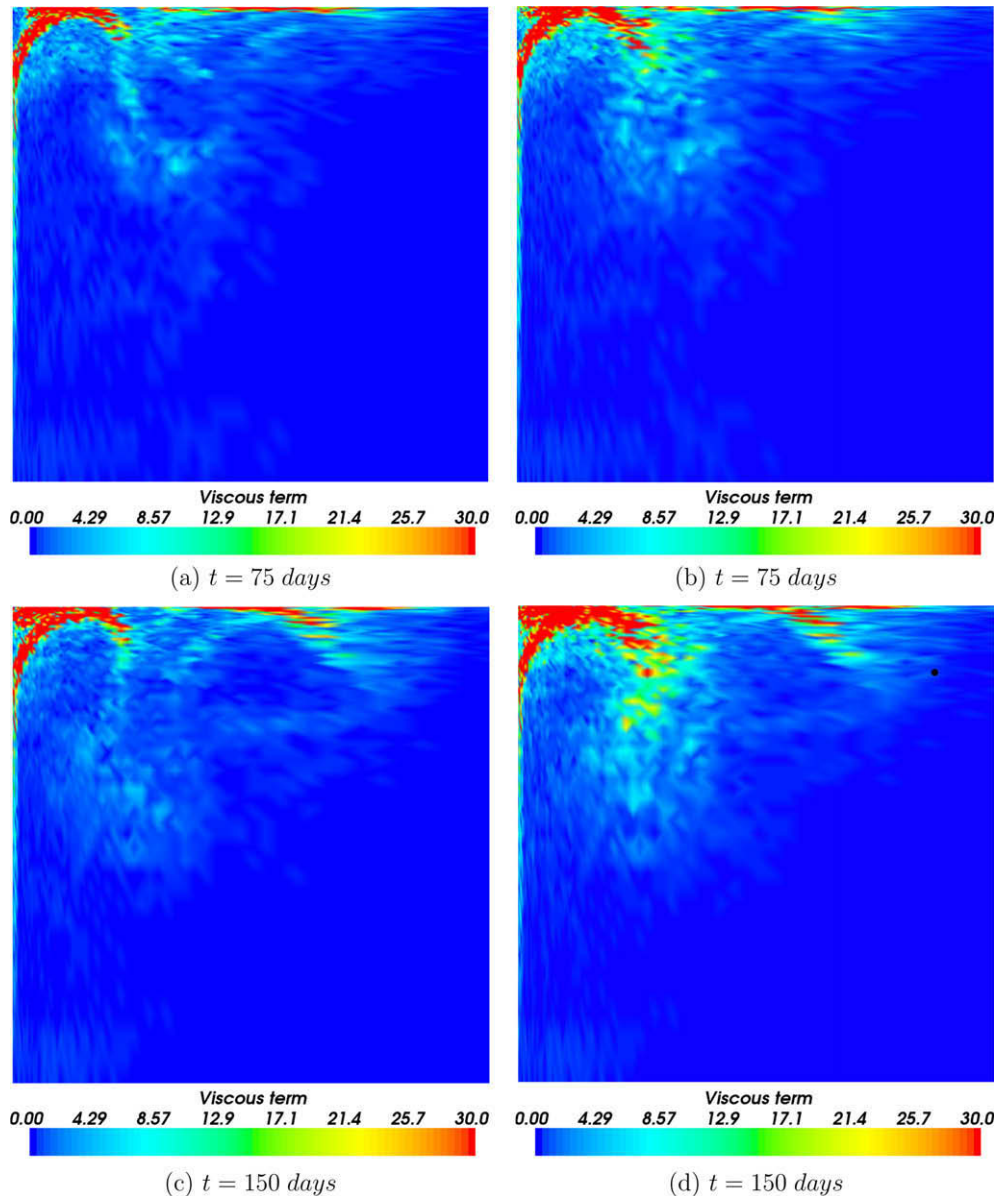


Fig. 9. Viscous forcing term from the full and POD reduced order models ($Re = 2000$; unit: N) at time levels: (a) and (b) $t = 75$ days; (c) and (d) $t = 150$ days; left panel: full model; right panel: POD model with the use of H^1 (201 snapshots and 100 POD bases are chosen).

4.2. Results and discussion

4.2.1. Test case I: $Re = 400–1200$

The case studies detailed below have been carried out with Reynolds numbers in the range 400–2000. It is noted that the POD-

Galerkin model with the L^2 norm can represent the velocity field well when $Re \leq 400$. In the case of $Re = 400$, 30 POD bases and 41 snapshots are chosen for velocity components u, v, w and pressure p , for which about 98.9% of energy is captured. The RMSE of velocity results between the POD and full models is less than

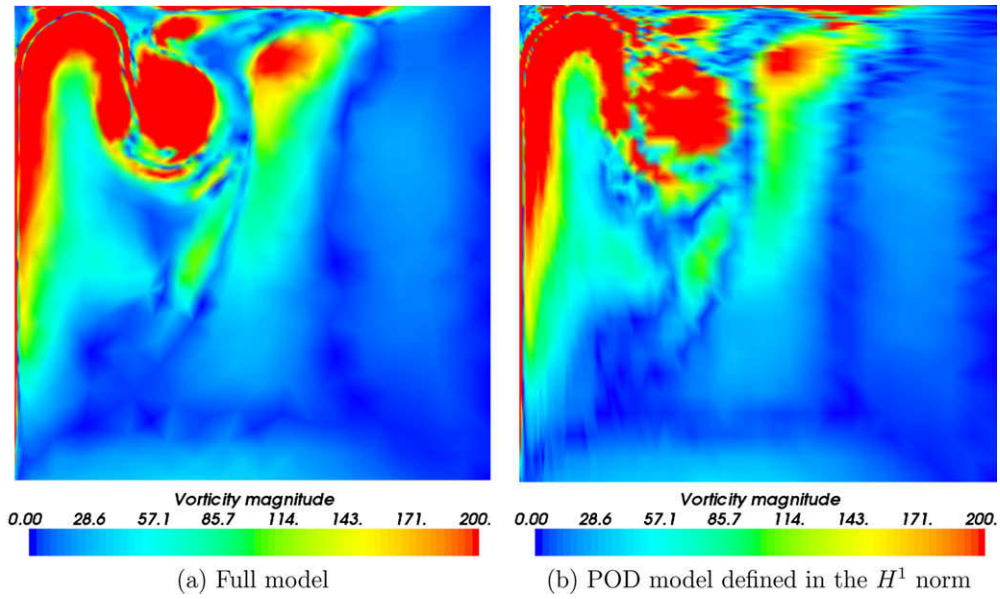


Fig. 10. Vorticity from the full and POD reduced order models ($Re = 2000$; unit: s^{-1}); at time level $t = 100$ days (a) full model; (b) POD model defined in the H^1 norm with 201 snapshots and 100 POD bases.

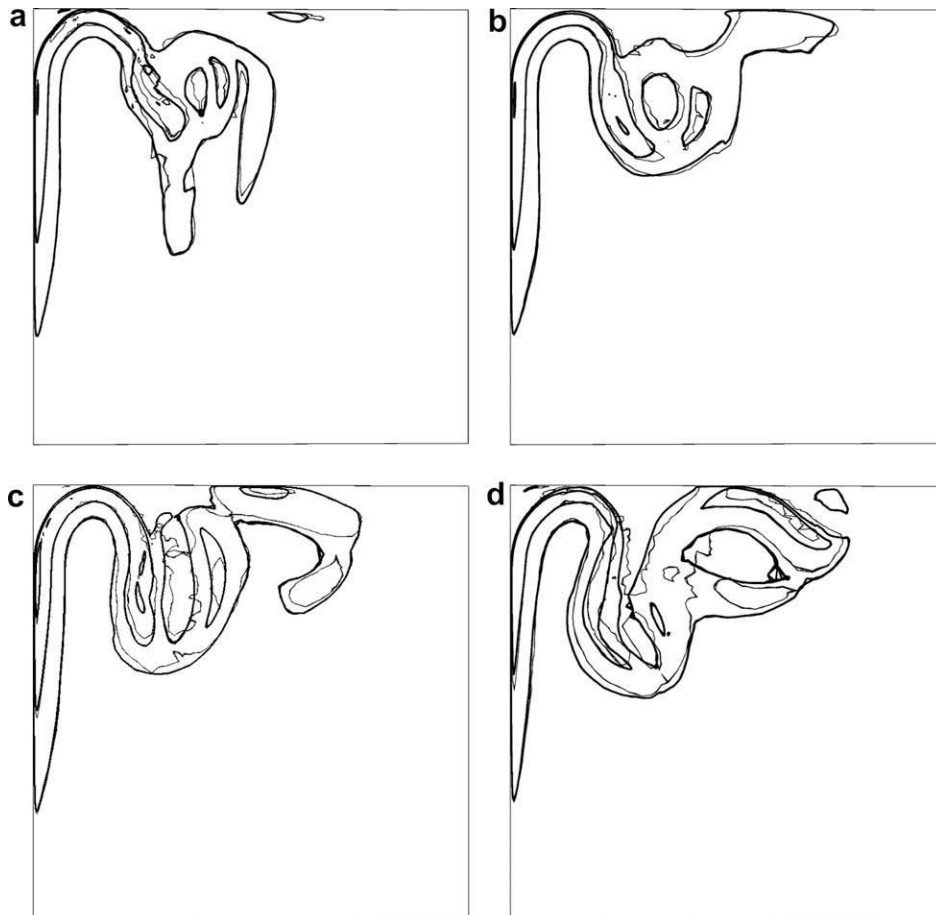


Fig. 11. Contours of velocity at time levels ($Re = 2000$): (a) $t = 62.5$ days; (b) $t = 75$ days; (c) $t = 87.5$ days; (d) $t = 100$ days (the thick lines: the full model; the thin lines: the POD model defined in H^1 . Two hundred and one snapshots and 100 POD bases are chosen).

3.5 m/s during the simulation period [50, 150] days. The POD-Galerkin model with the L^2 norm gradually lost its stability as the Reynolds number was further increased (i.e., $Re > 400$). There are two ways to stabilise the POD-ROM simulation:

- (1) Increasing the number of POD bases and snapshots.
- (2) Introducing artificial dissipation e.g. defining the POD basis in a Sobolev H^1 inner product norm.

For the cases ($Re = 800, 1200$), it is found that the velocity results can be represented better using the H^1 norm ($\epsilon = 0.00001$ for $Re = 800$ and $\epsilon = 0.00015$ for $Re = 1200$) than those using the L^2 norm. 41 snapshots with 30 POD bases was chosen for $Re = 800$ while the number of snapshots was increased to 81 with 70 POD bases for $Re = 1200$, where about 99.5% of energy was captured. The results from the POD reduced order model using the L^2 and H^1 norms are compared with corresponding results from the full model. The RMSE of velocity results between the POD and full models during the simulation period is provided in Fig. 2. It can be seen that by using the H^1 norm, the RMSE of velocity results between the POD and full models was reduced by up to 25% at $Re = 800$ (Fig. 2a) during the period $t = 100$ –150 days and by 50% at $Re = 1200$ (Fig. 2b) during the period $t = 80$ –120 days. The velocity contours for $Re = 1200$ are displayed in Fig. 3. It is observed that the instability in the POD velocity results is reduced by using the H^1 norm. Note that the coefficient ϵ is directly related to the accuracy of solutions in the POD model defined in H^1 (Fig. 4). One may guess ϵ is associated to Re (Iollo et al., 2000). Herein the value of the coefficient ϵ is 10^{-5} for $Re = 800$ and 1.5×10^{-4} for $Re = 1200$, respectively (where the average RMSE of velocity results over time reaches the minimum values, see Fig. 4).

To evaluate the interpolation error (introduced to snapshots and the POD reduced model), the comparison of POD results is carried out with linear and high order (quadratic and cubic) interpolation schemes. It can be seen (Fig. 5) that compared with that with the use of the linear interpolation, the RMSE of the velocity results (between the POD and full models) with the use of the quadratic and cubic interpolation schemes is reduced by 20–70%.

4.2.2. Test case II: $Re = 2000$

As the Reynolds number is further increased to 2000, the POD reduced order models defined in both the H^1 and L^2 norms become

oscillatory and unstable as the simulation time increases and the RMSE of velocity results increases to 9 m/s (Fig. 6a). The instability of the POD model can be reduced if the length of the integration period is shortened by half. The POD model is derived based on the snapshots obtained during the shortened period [50, 100] days. The RMSE of velocity results between the POD and full models is reduced by a factor of 2 after the simulation period is shortened (Fig. 6). With an increase in the number of snapshots and POD bases defined in the H^1 Sobolev norm, the RMSE of velocity is further decreased and attains a small value (less than 2 m/s, represented by the dot-dashed line in Fig. 6b). The effect of the truncation involved in the POD-Galerkin approach is further evaluated by the error of velocity results between the full and POD reduced order model defined in both the L^2 and H^1 norms (Fig. 7). By using the H^1 norm and increasing the number of snapshots and POD bases, the error in the velocity field decreases by 30–50% for the larger part of flow (Fig. 7) while the correlation of velocity results increases up to 97% (Fig. 8). By introducing a suitable artificial dissipation the viscous force magnitude ($\sqrt{(\mu \nabla^2 u)^2 + (\mu \nabla^2 v)^2}$, where μ is the kinematic viscosity) in the POD model is close to that in the full model (Fig. 9). A comparison of velocity results between the full model and POD model defined in H^1 (with 201 snapshots and 100 POD bases) is provided in Figs. 11 and 12 while the vorticity at time level $t = 100$ days is displayed in Fig. 10. Both the velocity and vorticity results from the POD model exhibit an overall good agreement with those obtained with the full model.

5. Summary and conclusions

The accuracy of POD-Galerkin model using adaptive meshes is investigated for moderate Reynolds numbers flows using the Munk gyre flow test case. A comparison of results between the full and POD-ROM models defined in both the L^2 and H^1 norms, has been carried out to evaluate the effect of the truncated modes when adaptive meshes are used in conjunction with POD. The results obtained show that the accuracy of the POD-Galerkin model can be improved by introducing an artificial dissipation using a Sobolev H^1 inner product norm when $Re = 800$ –2000. The RMSE of velocity results between the full model and POD-Galerkin model is reduced by 10–50% with the use of the H^1 norm. Both the velocity and vorticity results at the different time levels exhibit an overall good

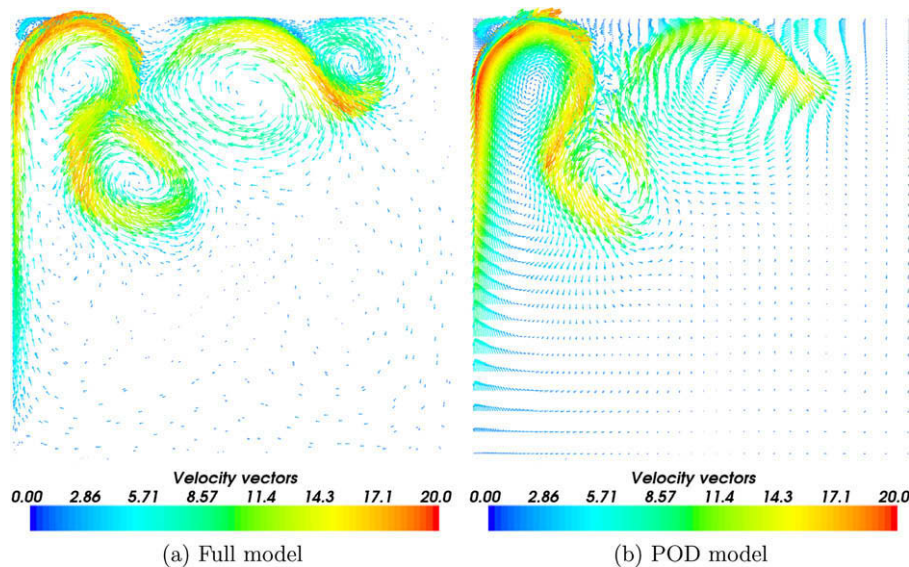


Fig. 12. Velocity field at time level $t = 150$ days ($Re = 2000$; unit: m/s): (a) full model; (b) POD model defined in H^1 with 201 snapshots and 100 POD bases are chosen.

agreement with those obtained with the full model. An increase in the number of snapshots and POD bases also leads to an improvement in the accuracy of the POD model (for example at $Re = 2000$, the RMSE of velocity results decreases to a small value (less than 2.5 m/s)).

Future work will investigate introducing calibration terms (e.g., eddy-viscosity terms) to the POD reduced order equations to account for unresolved fine-scale fluctuations in POD for higher Reynolds numbers of the order of $Re = 10,000$ (Bottaro et al., 2007; Favier et al., 2006; Noack et al., 2005; Stankiewicz et al., 2008; Pastoor et al., 2008). These calibration terms can be calculated by resolving appropriate constrained minimisation problems.

Acknowledgements

This work was carried out under funding from the UK's Natural Environment Research Council (projects NER/A/S/2003/00595, NE/C52101X/1 and NE/C51829X/1), the Engineering and Physical Sciences Research Council (GR/R60898) and the Leverhulme Trust (F/07058/AB), and with support from the Imperial College High Performance Computing Service and the Grantham Institute for Climate Change. Prof. I.M. Navon would like to acknowledge support of NSF grants ATM-0201808 and CCF-0635162. Finally the authors would like to thank the anonymous reviewers who assisted in substantially improving this paper.

References

- Aubry, N., Holmes, P., Lumley, J.L., 1988. The dynamics of coherent structures in the wall region of a turbulent boundary layer. *Journal of Fluid Dynamics* 192, 115–173.
- Cao, Y., Zhu, J., Luo, Z., Navon, I.M., 2006. Reduced order modeling of the Upper Tropical Pacific ocean model using proper orthogonal decomposition. *Computers and Mathematics with Applications* 52 (8–9), 1373–1386.
- Couplet, M., Basdevant, C., Sagaut, P., 2005. Calibrated reduced-order POD-Galerkin system for fluid flow modelling. *Journal of Computational Physics* 207, 192–220.
- Daescu, D.N., Navon, I.M., 2008. A dual-weighted approach to order reduction in 4D-Var data assimilation. *Monthly Weather Review* 136, 1026–1041.
- Fang, F., Pain, C.C., Piggott, M.D., Gorman, G.J., Goddard, A.J.H., 2005. An adaptive mesh adjoint data assimilation method applied to free surface flows. *International Journal for Numerical Methods in Fluids* 47 (8–9), 995–1001.
- Fang, F., Piggott, M.D., Pain, C.C., Gorman, G.J., Goddard, A.J.H., 2006. Adjoint data assimilation into a 3D unstructured mesh coastal finite element model. *Ocean Modelling* 15(3–38). doi:10.1016/j.ocemod.2006.05.001.
- Fang, F., Pain, C.C., Navon, I.M., Piggott, M.D., Gorman, G.J., Allison, P., Goddard, A.J.H., 2008a. Reduced order modelling of an adaptive mesh ocean model. *International Journal for Numerical Methods in Fluids*. doi:10.1002/flid.1841.
- Fang, F., Pain, C.C., Navon, I.M., Piggott, M.D., Gorman, G.J., Farrell, P.E., Allison, P., Goddard, A.J.H., 2008b. A POD reduced order 4D-Var adaptive mesh ocean modelling approach. *International Journal for Numerical Methods in Fluids*. doi:10.1002/flid.1911.
- Favier, J., Cordier, L., Kourta, A., Iollo, A., 2006. Calibrated POD reduced-order models of massively separated flows in the perspective of their control. In: Proceedings of 2006 ASME Joint US-European Fluids Engineering Summer Meeting, Miami, Florida, USA.
- Ford, R., Pain, C.C., Piggott, M.D., Goddard, A.J.H., de Oliveira, C.R.E., Umbleby, A.P., 2004. A nonhydrostatic finite-element model for three-dimensional stratified oceanic flows. Part I: model formulation. *Monthly Weather Review* 132 (12), 2816–2831.
- Fukunaga, K., 1990. *Introduction to Statistical Recognition*, second ed.. Computer Science and Scientific Computing Series Academic Press, Boston.
- Galletti, B., Bruneau, C.H., Zannetti, L., Iollo, A., 2004. Low-order modelling of laminar flow regimes past a confined square cylinder. *Journal of Fluid Mechanics* 503, 161–170.
- Galletti, B., Bruneau, C.H., Zannetti, L., Iollo, A., 2005. Accurate model reduction of transient flows. Technical Report, 5676, INRIA.
- Galletti, B., Bottaro, A., Bruneau, C.H., Iollo, A., 2007. Accurate model reduction of transient flows and forced wakes. *European Journal of Mechanics B/Fluids* 26 (3), 354–366.
- Gloerfelt, X., 2006. Compressible POD/Galerkin reduced-order model of self-sustained oscillations in a cavity. In: 12th AIAA/CEAS Aeroacoustics Conference (27th AIAA Aeroacoustics Conference), Cambridge, Massachusetts.
- Holmes, P., Lumley, J.L., Berkooz, G., 1998. *Turbulence, Coherent Structures, Dynamical Systems and Symmetry*. Cambridge University Press, Cambridge, UK.
- Hoteit, I., Kohl, A., 2006. Efficiency of reduced-order, time-dependent adjoint data assimilation approaches. *Journal of Oceanography* 62 (4), 539–550.
- Hussain, A.K.M.F., 1983. Coherent structures-reality and myth. *Physics of Fluids* 26 (10), 2816–2850.
- Iollo, A., Lanteri, S., Desideri, J.A., 2000. Stability properties of POD-Galerkin approximations for the compressible Navier–Stokes equations. *Theoretical and Computational Fluid Dynamics* 13, 377–396.
- Kirby, M., Sirovich, L., 1990. Application of the Karhunen–Loève procedure for the characterization of human faces. *IEEE Transactions on Pattern Analysis and Machine Intelligence* 12 (1), 103–108.
- Lumley, J.L., 1967. The structure of inhomogeneous turbulence. In: Yaglom, A.M., Tatarski, V.I. (Eds.), *Atmospheric Turbulence and Wave Propagation*. Nauka, Moscow, pp. 166–178.
- Luo, Z., Chen, J., Zhu, J., Wang, R., Navon, I.M., 2007a. An optimizing reduced order FDS for the tropical Pacific ocean reduced gravity model. *International Journal for Numerical Methods in Fluids* 45, 143–161.
- Luo, Z., Zhu, J., Wang, R., Navon, I.M., 2007b. Proper orthogonal decomposition approach and error estimation of mixed finite element methods for the tropical Pacific ocean reduced gravity model. *Computer Methods in Applied Mechanics and Engineering* 196, 4184–4195.
- Noack, B.R., Papas, R., Monkewitz, P., 2005. The need for a pressure-term representation in empirical Galerkin models of incompressible shear flows. *Journal of Fluid Mechanics* 523, 339–366.
- Pain, C.C., Piggott, M.D., Goddard, A.J.H., Fang, F., Gorman, G.J., Marshall, D.P., Eaton, M.D., Power, P.W., de Oliveira, C.R.E., 2005. Three-dimensional unstructured mesh ocean modelling. *Ocean Modelling* 10 (1–2), 5–33.
- Pastoor, M., Hennning, M., Noack, B.R., King, R., Tadmor, G., 2008. Feedback shear layer control for bluff body drag reduction. *Journal of Fluid Mechanics*. doi:10.1017/S0022112008002073.
- Rempfer, D., 2003. Low-dimensional modelling and numerical simulation of transition in simple shear flows. *Annual Review of Fluid Mechanics* 35, 229–265.
- Robert, C., Durbiano, S., Blayo, E., Verron, J., Blum, J., le Dimet, F.X., 2005. A reduced-order strategy for 4D-VAR data assimilation. *Journal of Marine Systems* 57 (1–2), 70–82.
- Sirovich, L., 1987. Turbulence and the dynamics of coherent structures. Part II: symmetries and transformations. *Quarterly of Applied Mathematics* 45, 573–582.
- Stankiewicz, W., Morzynski, M., Noack, B.R., 2008. Reduced order Galerkin models of flow around NACA-0012 airfoil. *Mathematical Modelling and Analysis* 13 (1), 113G–122G.
- Willcox, K., Peraire, J., 2002. Balanced model reduction via the proper orthogonal decomposition. *AIAA Journal* 40 (11), 2323–2330.